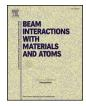
FISEVIER

Contents lists available at ScienceDirect

Nuclear Inst. and Methods in Physics Research B

journal homepage: www.elsevier.com/locate/nimb



GIFAD for He/KCl(001). Structure in the pattern for $\langle 110 \rangle$ incidence as a measure of the projectile-cation interaction



G.A. Bocan^{a,*,1}, M.S. Gravielle^{b,1}

- ^a Centro Atómico Bariloche, Av. Bustillo 9500, 8400 S.C. de Bariloche, Argentina
- b Instituto de Astronomía y Física del Espacio (IAFE, CONICET-UBA), Casilla de Correo 67, Sucursal 28, C1428EGA Buenos Aires, Argentina

ARTICLE INFO

Keywords: GIFAD He-KCl(001)

ABSTRACT

In this article we address grazing incidence fast atom diffraction (GIFAD) for the He/KCl(001) system, for which a systematic experimental study was recently reported [E. Meyer, Ph.D dissertation, Humboldt-Universität, Berlin, Germany, 2015]. Our theoretical model is built from a projectile-surface interaction obtained from Density Functional Theory (DFT) calculations and the Surface Initial-Value Representation (SIVR), which is a semi-quantum approach to describe the scattering process. For incidence along the $\langle 100 \rangle$ and $\langle 110 \rangle$ directions, we present and discuss the main features of our interaction potential, the dependence of the rainbow angle with the impact energy normal to the surface, and the simulated GIFAD patterns, which reproduce the main aspects of the reported experimental charts. The features of the diffraction charts for He/KCl(001) are related to the averaged equipotential curves of the system and a comparison is established with the case of He/LiF(001). The marked differences observed for $\langle 110 \rangle$ incidence are explained as due to the much larger size of the K⁺ ion relative to that of Li⁺.

1. Introduction

Grazing incidence fast atom diffraction (GIFAD) [1,2] is being rapidly incorporated to the set of surface analysis techniques. It shares with reflection high-energy electron diffraction (RHEED) the grazing incidence geometry, and complements thermal energy atom scattering (TEAS) [3] in the keV range just as RHEED does with low energy electron diffraction (LEED). GIFAD was first reported in 2007 [1,2] and its potential for nondestructive surface characterization was very early foreseen [4,5]. Furthermore, the extreme sensitivity of GIFAD to the projectile-surface interaction has positioned this technique as a powerful tool for probing potential energy surfaces (PES).

Incidence along or very close to high-symmetry directions is a requirement for the observation of non-specular scattering [6,7]. The GIFAD phenomenon takes place when atomic projectiles in the keV energy range grazingly impinge on a crystal surface along a low-index crystallographic direction. The scattering thus proceeds under axial surface channeling conditions [8]. The fast motion along the channel is, on a first approach, sensitive only to the periodic-PES average in this direction [9]. Hence, the associated energy E_{\parallel} is essentially conserved, and motions parallel and perpendicular to the channel get decoupled from each other. The scattering process can then be projected into the

plane normal to the channeling direction, with an associated energy $E_{\rm L}$ in a hyperthermal up to eV energy regime and a perpendicular De Broglie wavelength of the order of the interatomic spacing. Bragg diffraction out of the specular plane occurs whenever the transverse momentum transfer coincides with a reciprocal lattice vector. Such a transverse momentum exchange had already been proposed by Farías et al. [10] in 2004 to explain their observations for the scattering of $\rm H_2/Pd(111)$, at off-normal incidence with energies $E_i < 1$ eV.

The GIFAD pattern arises from the combination of two kinds of interference: a) interchannel interference, originated from the periodic array of channels, giving the Bragg peaks and b) intrachannel interference, originated from the corrugation of the interaction potential within a given channel, giving the rainbow peak as well as the supernumerary rainbows [11]. The result on the detection plane is typically a sequence of Bragg peaks whose intensities are modulated by the underlying intrachannel interference [11,12].

Although GIFAD has already been observed for a wide variety of surfaces, including semiconductors [4,13], metals [14,15], adsorbate-covered metals [5], ultra-thin films [16], organic molecules on metal substrates [17], etc., He/LiF(001) remains the benchmark system as the wide band-gap insulator character of LiF(001) together with the closed-shell electronic structure of He result in an efficient suppression of

^{*} Corresponding author.

E-mail address: gisela.bocan@cab.cnea.gov.ar (G.A. Bocan).

Also a member of Consejo Nacional de Investigaciones Científicas y Técnicas (CONICET).

electronic excitations [18]. Similar systems such as He/NaCl(001) [2], H/LiF(001) [1,2,19] or H/NaCl(001) [2] were examined as well in the early GIFAD experimental works, but so far they have not been as extensively studied [20–22]. In the present article we will address the ⁴He/KCl(001) system, the choice being strongly motivated by the experimental GIFAD diffraction charts recently reported by Meyer [23]. This system had previously been the subject of a rainbow-scattering theo-experimental study by Specht et al. [24,25], who analyzed the effect of the rumpling on the rainbow angle.

Our theoretical model for GIFAD is built from a high-precision interaction potential built from Density Functional Theory (DFT) calculations and a semi-quantum representation of the scattering process called the surface initial-value representation (SIVR) [26]. In this contribution we will use this model to simulate GIFAD for He/KCl(001). The focus of our analysis will be on i) the adequacy of our potential to reproduce the experimental GIFAD patterns [23]; and ii) the qualitatively different structure of the He/KCl(001) GIFAD pattern relative to that of He/LiF(001), particularly for incidence along the (110) direction.

We will show that simulated GIFAD patterns give a good accord with experiments for $\lambda_{\perp} \leq 0.6$ Å. Also we will explain the very different structure of the $\langle 110 \rangle$ chart, when compared with that of He/LiF(001), as arising from the much larger size of the K⁺ cation relative to that of Li⁺, resulting in the early presence of a double-well on the averaged equipotential curves. Noteworthily, a double-well shape had been predicted for H/LiF(001) by Rousseau et al. [19] based on the specific GIFAD patterns for that system. In a recent publication, we indeed observed that feature for H $\rightarrow \langle 110 \rangle$ LiF(001) [22].

This article is organized as follows: In Section 2 we briefly introduce the SIVR method and the interaction potential; in Section 3 we discuss the results concerning i) the features of the interaction potential, ii) the rainbow angle and iii) simulated diffraction charts. A comparison with He/LiF(001) is established in order to gain some insight into the nature of the projectile-cation interaction and how it affects the GIFAD pattern for incidence along the $\langle 110 \rangle$ direction. Finally in Section 4 we present our conclusions.

2. Theoretical model

2.1. Scattering process

We treat the scattering dynamics of He atoms grazingly colliding with the KCl(001) surface by means of the SIVR model [26,27]. This semi-quantum approach is based on the Initial Value Representation (IVR) method by Miller [28], which represents a practical way of introducing quantum effects, such as interferences and classical forbidden processes, in classical dynamics simulations [29]. The basic idea of IVR is, within the Feynman path integral formulation, to replace the fullquantum time evolution operator by the Van Vleck propagator in terms of classical trajectories with different initial conditions. This evolution operator is then evaluated numerically without any further approximation. The SIVR model uses the IVR time evolution operator in the frame of a time-dependent distorted-wave formalism. In accord with a full-quantum treatment, a smooth maximum is obtained at the classical rainbow angle, which exponentially decays on the classical forbidden region. The SIVR method provides an appropriate description of GIFAD patterns along the whole angular range and can be considered as an attractive alternative to quantum wave packet propagations, offering a clear representation of the main mechanisms of the GIFAD process. The interested reader can find a more detailed discussion of the SIVR model in Refs. [22,26,27].

Regarding the present calculation, notice that SIVR projectile distributions are sensitive to the size of the surface region that is coherently illuminated by the incident beam, and this size depends on the collimating setup [27,30,31]. In this work we assume a coherently illuminated square region covering two equivalent parallel channels of the surface lattice, i.e., we use transverse coherent lengths $\sigma_x = \sigma_y = 2a_y$

in Eq. (7) from Ref. [31], where a_y is the half-width of the incidence channel. The angular dispersion was derived from these parameters by using Eq. (10) from Ref. [31] considering an impact energy E=2 keV. The resulting azimuthal divergence of the incident beam ranges between 0.01 and 0.02 deg, being in accord with the experimental value that is smaller than 0.03 deg [25]. In connection with this it should be mentioned that GIFAD experiments also involve inelastic processes [32], which are not included in our model and might affect the spectra. In addition, the starting point of the classical projectile trajectories was chosen at the normal position $Z_0=1.4\ a$ (a is the lattice constant) relative to the surface, thus ensuring a negligible projectile-surface interaction.

2.2. Projectile-surface potential

The He-KCl(001) potential was obtained from DFT calculations, performed with the QUANTUM ESPRESSO code [33]. The procedure was analogous to the one discussed for H-LiF(001) in Ref. [22]. In this section we briefly present its main features.

The PES is three-dimensional (3D) and is built out of a selection of 6 high-symmetry (X_i, Y_i) configurations and 20 Z_i values (Z = 0 falls on the topmost Cl layer), by means of a three-dimensional interpolation technique, which makes use of cubic splines and the corrugation reducing procedure (CRP) [34].

For the DFT calculations, we use projector augmented-wave (PAW) pseudopotentials [35,36] to describe the electron-core interaction, while for the exchange–correlation functional we consider the generalized gradient approximation (GGA), with the Perdew-Burke-Ernzerhof (PBE) functional [37]. Thus, we will hereafter refer to the resulting interaction potential as a PAW-PBE PES.

The DFT calculations are performed with an energy cutoff in the plane-wave expansion of 80 Ryd for the wave functions and 320 Ryd for the charge density and potential. A $2 \times 2 \times 1$ Monkhorst–Pack grid of special k-points is used for the Brioullin-zone integration. The KCl lattice constant is a=6.381 Å, slightly higher than the experimental value of 6.28 Å [38].

We represent the KCl(001) surface by means of the supercell-slab scheme. The supercell consists of a $\sqrt{2} \times \sqrt{2}$ surface cell, a six-layer slab and a vacuum distance of $6d=3\frac{a}{2}\sim 9.6$ Å. The relaxed surface equilibrium geometry presents a *rumpling*, defined as the half-distance between relaxed Cl and K planes. For the topmost Cl and K planes, we get a rumpling of +0.025 Å, with Cl atoms moving outward and K atoms moving inward. This value is consistent with LEED experiments which yield a rumpling of 0.03 ± 0.05 Å [38] and compares very well with Specht's 0.03 Å [24], obtained from a vdW-D2 calculation (PBE plus semiempirical dispersion corrections [39]).

The geometry of GIFAD for He/KCl(001) as well as the channeling directions $\langle 110 \rangle$ and $\langle 100 \rangle$ are illustrated in Fig. 1.

3. Results and discussion

3.1. The potential energy surface

GIFAD is extremely sensitive to the projectile-surface interaction, particularly to the profile and corrugation of the PES near the reflection region. Our PES is 3D and no dimension reduction is made during the dynamics. However, the fast motion of the projectile along the channel is in fact mainly ruled by the average interaction in this direction and thus we will discuss the PES features in these terms.

In Fig. 2a and b we consider the energy averages respectively along the $\langle 100 \rangle$ and $\langle 110 \rangle$ channels, and depict equipotential contours across them. Across a $\langle 100 \rangle$ channel, the equipotential curves have only one maximum at the border of the channel, corresponding to the rows of alternating Cl $^-$ and K $^+$ ions. In contrast, across a $\langle 110 \rangle$ channel the equipotential curves have local maxima both at the border and at the middle of the channel, respectively corresponding to the rows of Cl $^-$

Download English Version:

https://daneshyari.com/en/article/8039251

Download Persian Version:

https://daneshyari.com/article/8039251

Daneshyari.com